An integrated WRF/HYSPLIT modeling approach for the assessment of PM$_{2.5}$ source regions over the Mississippi Gulf Coast region

Anjaneyulu Yerramilli · Venkata Bhaskar Rao Dodla · Venkata Srinivas Challa ·
LaToya Myles · William R. Pendergrass · Christoph A. Vogel · Hari Prasad Dasari ·
Francis Tuluri · Julius M. Baham · Robert L. Hughes · Chuck Patrick ·
John H. Young · Shelton J. Swanier · Mark G. Hardy

Abstract Fine particulate matter (PM$_{2.5}$) is majorly formed by precursor gases, such as sulfur dioxide (SO$_2$) and nitrogen oxides (NO$_x$), which are emitted largely from intense industrial operations and transportation activities. PM$_{2.5}$ has been shown to affect respiratory health in humans. Evaluation of source regions and assessment of emission source contributions in the Gulf Coast region of the USA will be useful for the development of PM$_{2.5}$ regulatory and mitigation strategies. In the present study, the Hybrid Single-Particle Lagrangian Integrated Trajectory (HYSPLIT) model driven by the Weather Research & Forecasting (WRF) model is used to identify the emission source locations and transportation trends. Meteorological observations as well as PM$_{2.5}$ sulfate and nitric acid concentrations were collected at two sites during the Mississippi Coastal Atmospheric Dispersion Study, a summer 2009 field experiment along the Mississippi Gulf Coast. Meteorological fields during the campaign were simulated using WRF with three nested domains of 36, 12, and 4 km horizontal resolutions and 43 vertical levels and validated with North American Mesoscale Analysis. The HYSPLIT model was integrated with meteorological fields derived from the WRF model to identify the source locations using backward trajectory analysis. The backward trajectories for a 24-h period were plotted at 1-h intervals starting from two observation locations to identify probable sources. The back trajectories distinctly indicated the sources to be in the direction between south and west, thus to have origin from local Mississippi, neighboring Louisiana state, and Gulf of Mexico. Out of the eight power plants located within the radius of 300 km of the two monitoring sites examined as sources, only Watson, Cajun, and Morrow power plants fall in the path of the derived back trajectories. Forward dispersions patterns computed using HYSPLIT were plotted from each of these source locations using the hourly mean emission concentrations as computed from past annual emission strength data to assess extent of their contribution. An assessment of the relative contributions from the eight sources reveal that only Cajun and Morrow power plants contribute to the observations at the Wiggins Airport to a certain extent while none of the eight power plants contribute to the observations at Harrison Central High School. As these observations represent a moderate event with daily average values of 5–8 µg m^{-3} for sulfate and 1–3 µg m^{-3} for HNO$_3$ with differences between the two spatially varied sites, the local sources may also be significant contributors for the observed values of PM$_{2.5}$.

A. Yerramilli (✉) · V. B. R. Dodla · H. P. Dasari · F. Tuluri ·
J. M. Baham · R. L. Hughes · C. Patrick · J. H. Young ·
S. J. Swanier · M. G. Hardy
Trent Lott Geospatial and Visualization Research Center, College
of Science Engineering and Technology, Jackson State University,
Jackson, MS 39217, USA
e-mail: yerramilli.anjaneyulu@jsums.edu

L. Myles · W. R. Pendergrass · C. A. Vogel
Air Resources Laboratory,
Atmospheric Turbulence & Diffusion Division, NOAA,
Oak Ridge, TN, USA

V. S. Challa
Radiological Safety Division,
Indira Gandhi Centre for Atomic Research,
Kalpakkam, 603102, India

Introduction

The Mississippi coastal zone along the Gulf of Mexico is experiencing multiple air pollution problems as a consequence of increased growth of industrial activities like oil and gas development and thermal power plants. Modeling studies on the atmospheric dispersion of air pollutants for assessing their spatiotemporal distributions under varied meteorological conditions will be useful for air quality risk assessment and development of emission regulations. Coastal regions are particularly complex as topographic variations and land–sea interactions influence the local flow, and the resultant mesoscale circulations influence the pollutant dispersion (Pielke et al. 1991; Lu and Turco 1995). Mesoscale atmospheric models are widely used to capture the complex flow and meteorological parameters essential in dispersion estimations over complex terrain (Physick and Abbs 1991; Kotroni et al. 1999; Wang and Ostoja-Starzewski 2004). Sulfur dioxide (SO_2) concentrations from major elevated sources in southern Florida were studied with a coupled dispersion model by Segal et al. (1988), which showed that local sea-breeze circulations led to complex dispersion patterns leading to higher concentrations. Moran and Pielke (1996) used a coupled mesoscale atmospheric and dispersion modeling system for tracer dispersion over complex topographic regions. Jin and Raman (1996) studied dispersion from elevated releases under the sea–land breeze flow using a mesoscale dispersion model which included the effects of local topography, variability in wind, and stability. Draxler (2006) used the Hybrid Single-Particle Lagrangian Integrated Trajectory (HYSPLIT) model to predict transport and dispersion of trace plumes over Washington, DC. Myles et al. (2009) reported that sulfur and nitrogen oxides react in the atmosphere to form compounds which may be transported over long distances and subsequently deposited as particulate matter. Anjaneyulu et al. (2008, 2009) and Challa et al. (2008, 2009) have studied the atmospheric dispersion over the Mississippi Gulf Coast region using an integrated mesoscale weather prediction and atmospheric dispersion model.

The Mississippi Gulf Coast is a typical coastal urban terrain featuring several industries that have been identified as emission sources of $PM_{2.5}$ and its precursor gases. $PM_{2.5}$ is a mixture of solid and liquid atmospheric particles (≤ 2.5 μm aerodynamic diameter) which mainly originate from anthropogenic sources like thermal power plants, fossil fuel burning, automobile emissions, smelting, and metal processing. Fine particulates $PM_{2.5}$ are mainly formed by condensation of gaseous precursors like SO_2, nitrogen oxides (NO_x), and volatile organic compounds (VOCs) which constitute a major portion of total $PM_{2.5}$ in ambient atmosphere, particularly in the

southeastern USA (Parkhurst et al. 1999; Weber et al. 2003).

In this work, a numerical modeling approach has been adopted to examine the atmospheric dispersion of SO_2 and NO_x (secondary species of $PM_{2.5}$) from elevated point sources in the Mississippi Gulf Coast region and no biogenic sources are considered (Chen et al. 2002). The dispersion of SO_2 and NO_x was computed separately as they are the precursors of $PM_{2.5}$ forming sulfate and HNO_3. The HYSPLIT model (Draxler and Hess 1997) was used to simulate dispersion in the coastal environment. Meteorological fields for the study period were predicted with the Advanced Research version of the Weather Research and Forecasting (ARW WRF) mesoscale model (Skamarock et al. 2008). In situ $PM_{2.5}$ sulfate and nitric acid (HNO_3) concentrations were collected at two sites during the Mississippi Coastal Atmospheric Dispersion Study, a joint Jackson State University Trent Lott Geospatial Visualization Research Center and NOAA Air Resources Laboratory summer field experiment in 2009 near Gulfport, MS, USA. The present study is an attempt to identify the potential emission sources which fall in the track of the HYSPLIT back trajectories under the given meteorological conditions, and to determine the extent of their relative contribution using the forward dispersion patterns to the observed concentrations at the two sites where field measurements were made.

Methodology

Description of models

The Advanced Research version of WRF (ARW) was used to produce atmospheric fields at a high resolution over the study region. ARW uses fully compressible, non-hydrostatic equations, terrain following vertical coordinates, and staggered horizontal grids. The model has several options for spatial discretization, diffusion, nesting, lateral boundary conditions, and parameterization schemes for sub-grid scale physical processes. The physics consists of microphysics, cumulus convection, planetary boundary layer turbulence, land surface, and longwave and shortwave radiation (Skamarock et al. 2008). ARW is suitable for use in a broad range of applications across scales ranging from meters to thousands of kilometers.

HYSPLIT 4.9 was used to compute simple air parcel trajectories as well as dispersion and deposition simulations. HYSPLIT computes the advection of a single pollutant particle, or simply its trajectory. The dispersion of a pollutant is calculated by assuming either puff or particle dispersion. In the puff approach, puffs expand until they exceed the size of the meteorological grid cell (either horizontally or vertically)

and then split into several new puffs, each with its share of the pollutant mass. In the particle approach, a fixed number of initial particles are advected about the model domain by the mean wind field and a turbulent component. The turbulent component of particle motion is computed by an autocorrelation function based on Lagrangian time scale and a computer-generated random number (Draxler and Hess 1997, 1998; Draxler and Rolph 2010).

Numerical simulations

In the present study, the ARW mesoscale atmospheric model and the HYSPLIT air quality and dispersion model were integrated to identify emission sources using backward trajectories and then computing the forward dispersion of pollutants from the source location. The ARW model was used with three domains, where the outer domain covered a fairly large region of the southeastern USA and the inner third domain covered the Mississippi Gulf Coast and parts of Louisiana and Alabama at 4-km fine resolution (Fig. 1). The model was designed to have three two-way interactive nested domains, centered at 32.8°N, 86.5°W with Lambert Conformal Conic (LCC) projection. Grid spacing for domains 1, 2, and 3 were taken as 36 km, 12 km, and 4 km, with grid sizes of 54×40, 109×76, and 187×118 points in the east–west and north–south directions, respectively. A total of 43 vertical levels were considered in the model, of which 33 levels are placed below 500 hPa for better simulation of the boundary layer flow characteristics. Terrain, land use, and soil data were interpolated to the model grids from US Geological Survey global elevations, vegetation category data, and FAO (Food and Agricultural Organization) soil data with suitable spatial resolution for each domain (5′, 2′, and 30″ for domains 1, 2, and 3, respectively) to define lower boundary conditions. Model physics included WSM3 simple microphysics scheme (Hong et al. 2004), Kain–Fritsch cumulus parameterization scheme (Kain and Fritsch 1993) on outer domains 1 and 2, Dudhia scheme for shortwave radiation (Dudhia 1989) and RRTM (Rapid Radiative Transfer Model) scheme for longwave radiation (Mlawer et al. 1997), the YSU (Yonsei University) non-local diffusion scheme (Hong et al. 2006), and the NOAH land surface model (Chen and Dudhia 2001) for surface processes. The model was integrated continuously for 48 h starting from 00 UTC of 16, 17, and 18 June, 2009 and without nudging. In each case, the first 24 h of simulation was treated as warm-up period and the simulations from
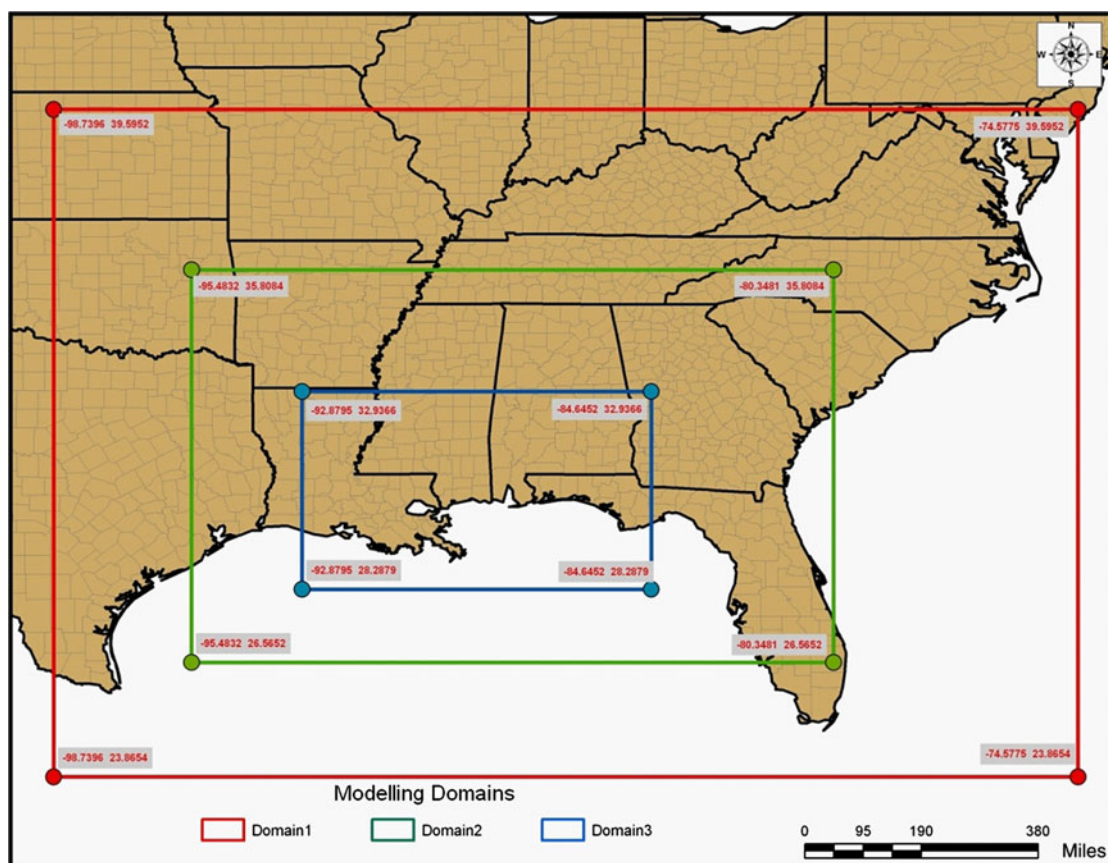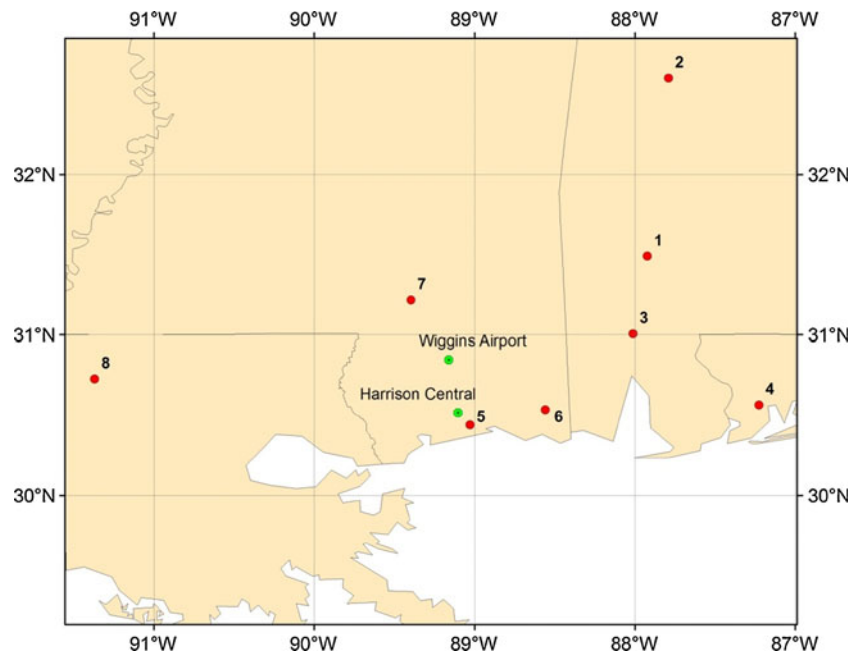

Fig. 1 WRF model domains

Fig. 2 Locations of the two observations sites of PM2.5 sulfate and HNO3 (*green circles*) over the Mississippi Gulf Coast region along with the coal-fired power plants (*red circles*) within a 300-km radius of the observation sites

00 to 23 UTC of 17, 00–23 UTC of 18, and 00–01 UTC of 19, June 2009 were considered for the analysis from the three integrations, respectively. Initial and boundary conditions were adopted from National Centers for Environmental Prediction Final Analyses (NCEP FNL) data available at 1° horizontal resolution. Boundary conditions were updated at 6-h intervals during the period of model integration.

HYSPLIT model was driven by simulated atmospheric fields to produce back trajectories of parcels originating from an observation site. The back trajectories provide the Lagrangian path of the air parcels in the chosen time scale (24 h in the present study), which will be useful to identify the source locations of the pollutant that fall in the track of the back trajectories. Integrated measurements of $PM_{2.5}$ SO_4 and HNO_3 concentrations collected during 17–20 June 2009 at the two observation sites, Harrison Central High School (HCHS) and Wiggins/Stone County Airport (WSAP), are used for back trajectory analysis. Possible emission sources were identified from the back trajectory paths.

Once the sources were identified, HYSPLIT model was used to produce forward dispersion patterns of the pollutants from each of the identified source locations for a 24-h period using US Environmental Protection Agency (US EPA) emission data and US Energy Information Administration's inventory data. The computational domain in HYSPLIT was designed with a horizontal grid of 300× 300 cells each of 0.05° resolution and with eight vertical levels (50, 100, 200, 500, 1,000, 2,000, and 5,000 m above ground level). A full 3-D particle model of dispersion was used with a total of 5,000 particles released for every emission cycle. The horizontal and vertical turbulence velocities are calculated with the Kantha and Clayson (2000) method. The boundary layer stability was estimated using the heat and momentum fluxes, and the mixed layer depth was taken from the meteorological model. The forward atmospheric dispersion characteristics of the pollutants from each of the power plants were analyzed to assess their relative contributions to the observed values at the monitoring sites.

Table 1 Measured concentrations of $PM_{2.5}$ sulfate and HNO_3 at Harrison (HCHS) and Wiggins (WSAP)

Date/start time (CST)	Date/end time (CST)	HCHS HNO_3 ($\mu g\ m^{-3}$)	HCHS $PM_{2.5}$ sulfate ($\mu g\ m^{-3}$)	WSAP HNO_3 ($\mu g\ m^{-3}$)	WSAP $PM_{2.5}$ sulfate ($\mu g\ m^{-3}$)
6/17/2009 14:00	6/17/2009 20:00	3.14	8.38	1.76	5.94
6/17/2009 20:00	6/18/2009 20:00	2.34	6.78	1.64	7.61
6/18/2009 20:00	6/19/2009 20:00	3.07	6.71	2.80	5.46
6/19/2009 20:00	6/20/2009 14:00	3.01	5.87	–	–
6/19/2009 20:00	6/20/2009 08:00	–	–	2.65	6.77

PM$_{2.5}$ precursor gas reactions

Ambient PM$_{2.5}$ in the southeastern region of the USA contains, apart from carbonaceous material, significant amounts of sulfates and nitrates which are of secondary origin, according to the United States Environmental Protection Agency (2004). The formation of aerosol sulfates and nitrates which contribute to PM$_{2.5}$ takes place through very complex atmospheric chemistry oxidation processes. The concentrations of gaseous precursors, such as SO$_2$ and NO$_x$, and oxidants, such as ozone, in the ambient air and meteorological factors, such as temperature, humidity, wind speed, and wind direction, determine the actual chemical formation pathways. The various thermodynamically feasible competing pathways and potentially limited reactant availabilities at many of the steps in the oxidation processes and the ambient meteorological conditions will determine the complexity of the atmospheric reactions in the secondary particulate formation (Zhang et al. 2009). Many of the sources for secondary particulate matter may not be local, but from regional sources such as thermal power plants, which are known to be significant contributors of gaseous precursors. Besides power plants, emissions from area sources, mobile sources biomass burning, etc. also contribute to the sulfate aerosols.

Description of in situ measurements

Integrated measurements of PM$_{2.5}$ sulfate and nitric acid were taken at two sites, HCHS (30.5°N, 89.1°W) and WSAP (30.8°N, 89.13°W). The locations of these two observation sites are shown in Fig. 2. At each site, annular denuder systems (URG Corp., Chapel Hill, NC, USA) were deployed at heights of 1.5 m for 6-h sampling periods beginning at 0200, 0800, 1400, and 2000 CST (Table 1). The sample flow rate was 20 L min^{-1} through 1% sodium carbonate in 2% glycerin in methanol-coated annular denuders (242 mm length) to capture HNO$_3$. Whatman® PTFE membrane filters were used in the dual-stage filter packs to collect PM$_{2.5}$ sulfate. Annular denuders were extracted with 10 mL of deionized water, and filters were extracted with 15 mL of a 90% deionized water/10% methanol solution. Samples were analyzed with a Metrohm 790 Personal Ion Chromatography System (Herisau, Switzerland). Concentrations obtained from in situ measurements at HCHS and WSAP were used to compute average concentration daily values as representative on each day of the sampling period (17–20 June 2009).

Results and discussion

The time series of concentrations of PM$_{2.5}$ sulfate and HNO$_3$ at Harrison and Wiggins are presented in Fig. 3 and
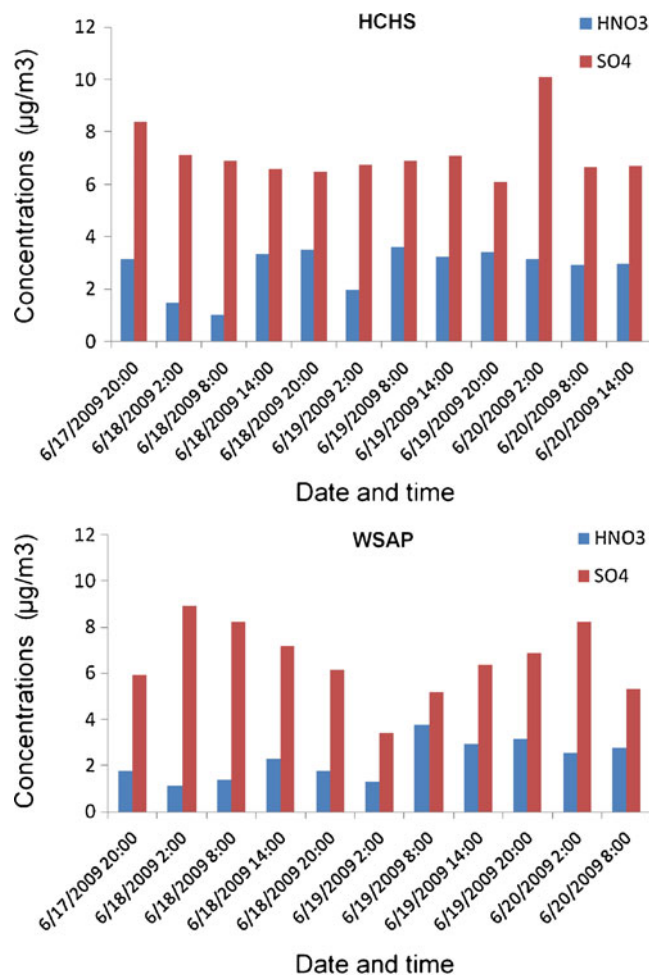

Fig. 3 Time series of HNO$_3$ and PM$_{2.5}$ sulfate concentrations at HCHS and WSAP (time is in US CST

corresponding 24-h average concentration values are given in Table 1. These data indicate that the magnitudes of average concentrations are in the range of 5–8 μg m^{-3} for sulfate as compared to 1.5–3 μg m^{-3} for HNO$_3$. In comparison, the background concentrations for PM$_{2.5}$ for eastern US are reported as 2.5 μg m^{-3} (http://www.epa.gov/ttn/naaqs/standards/pm/data/langstaffmemo2005.pdf) while for the southeast USA (mainly Texas state data) annual averages of daily average PM$_{2.5}$ concentrations range between 10 and 15 μg m^{-3} (the National Ambient Air Quality Standard is 15 μg m^{-3}; Allen 2002; http://eosweb.larc.nasa.gov/PRODOCS/narsto/document/EPA_SS_Houston_Final_Report.pdf). In the above studies, they have reported an average, sulfate accounts for approximately 30% of fine particulate mass (this fraction is variable on a daily basis; the average sulfate fraction is relatively independent of total PM$_{2.5}$ mass) while nitrate accounts for about 5% of sulfate.

In the present study, although data is available for three consecutive days between 1400 CST of 17 June

2009 and 1400 CST of 20 June 2009, model simulations were carried out to study only the 1-day period between 0100 UTC of 18 June 2009 to 0100 UTC of 19 June 2009 (to correspond with observation times of 2000 CST of 17 June 2009 to 2000 CST of 18 June 2009). The ARW mesoscale model was integrated starting at 0000 UTC of each day of 16–18 June 2009 to simulate the atmospheric fields for the period from 00 to 23 UTC of 17 June 2009; 00–23 UTC of 18 June 2009 and 00–01 UTC of 19 June 2009 discarding the first 24-h model outputs as corresponding to warm-up period as described in "Methodology". Model-derived high resolution (4 km) atmospheric fields at 1-h time interval were provided as input to the HYSPLIT model for computing back trajectories for source identification and for generating forward atmospheric dispersion patterns for assessing extent of contribution of each source. During the observation period, daily maximum temperatures over Mississippi Gulfport region were higher than normal with values around 36–37°C and heat wave conditions were reported by NOAA's National Weather Service.

Model-simulated wind regime

ARW model integrations provided three-dimensional meteorological fields (wind, temperature, and humidity) over the model domains at 1-h time interval that are necessary to drive the HYSPLIT model for computing back trajectories and forward dispersion. Model-simulated atmospheric flow fields are validated by comparison with the North American Mesoscale (NAM)-12 km regional analysis only as they are critically important for computation of back trajectories and forward dispersion. Evaluation of ARW model simulations of temperature, humidity, and wind fields and sensitivity experiments with different parameterizations of planetary boundary layer and land surface physics with the same model configuration for this study period was performed as a part of another study (Pendergrass et al. 2010a, b) which have shown that the model simulations are good up to 48 h and the schemes of YSU PBL and NOAH land-surface physics as used in this study provide the best simulation of PBL structure. The ARW model-simulated wind flow at 10 m above ground corresponding to two synoptic times of 0600 and 1800 UTC on 18 June are analyzed to understand
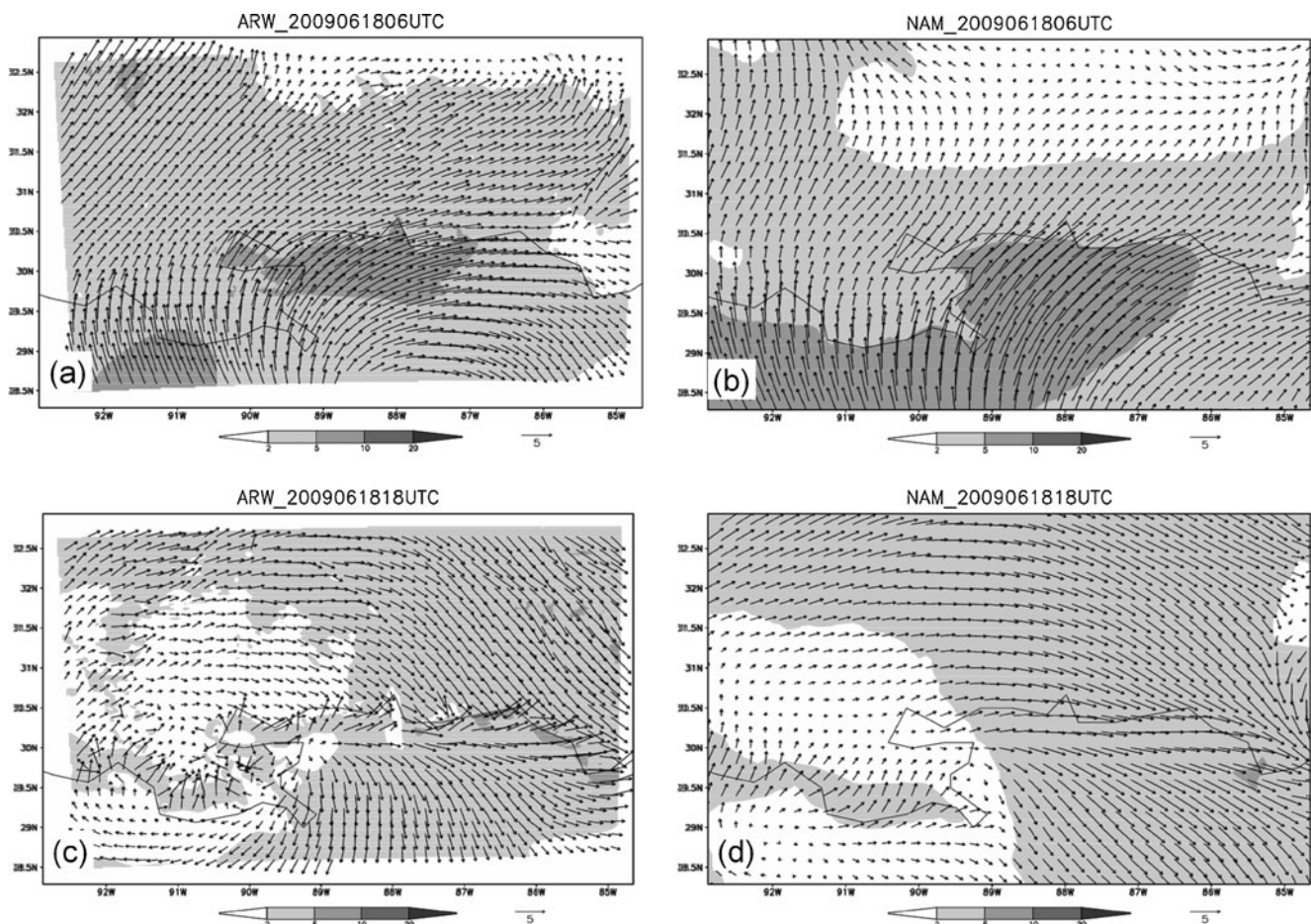

Fig. 4 Model-simulated (*left panel*) and NAM-12 analysis (*right panel*) wind flow at 10 m above ground over the study region corresponding to **a** 0100 CST (0600 UTC) and **b** 1300 CST (1800 UTC) on 18 June 2009
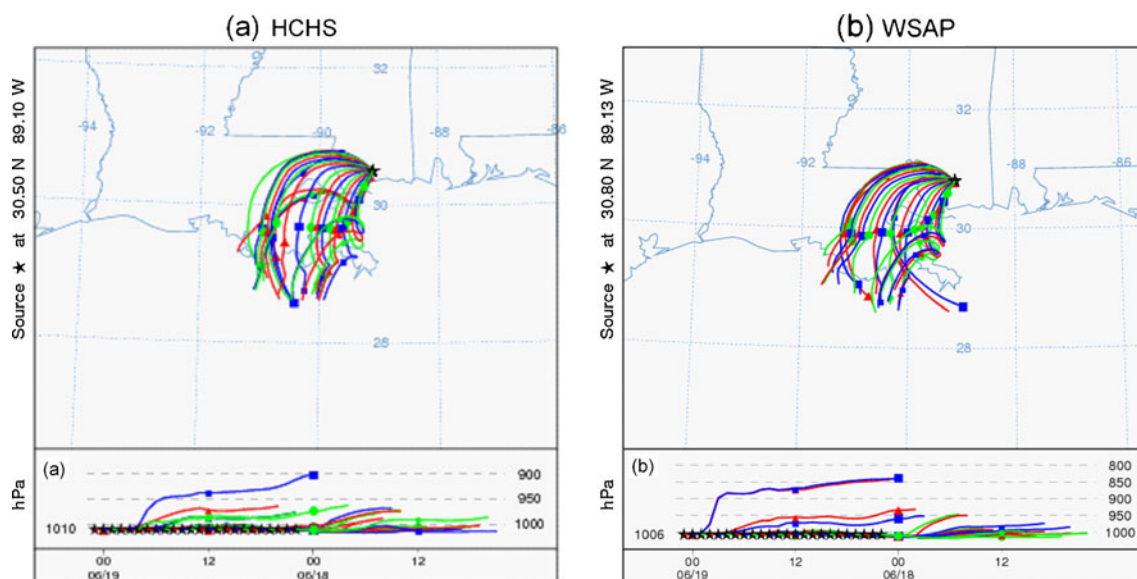
Fig. 5 Computed back trajectories at 1-h intervals for the 24-h period ending 0100 UTC on 19 June 2009 from the observation sites at **a** HCHS (*left*) and **b** WSAP (*right*). *Top portion* shows the horizontal path, and the *bottom portion* shows the vertical path of the trajectories

the prevailing surface wind flow regimes during the study period and compared with NAM regional analyses at 12-km resolution for validation (Fig. 4). NAM-12 km analysis is available in real time through NOAA (National Oceanic and Atmospheric Administration) NOMADS (National Operational Model Archive and Distribution System) (http://nomads.ncdc.noaa.gov). The simulated wind flow pattern shows clockwise circulation over the study region, indicating the presence of a high pressure system near the surface. At 0600 UTC (0100 CST) on 18 June, winds were southerly/southwesterly over the southwest/northwest of model domain, and assume a more westerly component over eastern parts resulting in a clear clockwise turning over southeast parts of the model domain all under the influence of a high pressure system. The strength of the wind flow was 2–5 m s^{-1} over most of the domain and greater than 5 m s^{-1} over small ocean regions adjoining the

Mississippi (MS) and Louisiana Gulf Coast regions. These stronger winds are constrained to the ocean region due to the influence of land breeze. At 1800 UTC (1300 CST), model-simulated wind flow shows clockwise circulation with the ridge line along 30 N near the Louisiana coast. The divergent flow emanating from this divergence center is indicated as easterlies over ocean region of the southwest parts, turning clockwise to become southerlies over western parts, westerlies over central north, northwesterlies over northeast parts, and northerlies over southeastern parts of the model domain. The wind flow was weaker (2–5 m s^{-1})/ stronger (5–10 m s^{-1}) over western/eastern parts indicating the divergence center over western parts of the model domain. Evidence of the onset of sea breeze is seen along the coastal regions with stronger wind flow (5–10 m s^{-1}) directed towards land. These model-simulated features agree with NAM-12 km analysis both in terms of strength

Table 2 List of identified coal-fired power plant sources, their locations, and annual emission values of SO$_2$ and NO$_x$ in tons (based on US EPA 2006 data)

S. no.	Name	Latitude °N	Longitude °W	Annual emission of SO$_2$ (tons)	Annual emission of NO$_x$ (tons)
1	Charles R. Lowman Power Plant, Leroy, AL 36548	31.489833	87.9215	17,878	10,881
2	Green County Steam Plant, Forkland, AL 36740	32.6025	87.7889	37,863	6,518
3	Barry Steam Plant, Bucks, AL 36512	31.0059	88.011383	52,621	16,800
4	Crist Plant, Pensacola, FL 32520	30.565167	87.225944	35,614	6,739
5	Jack Watson Generating Plant, Gulfport, MS 39502	30.439444	89.026667	29,113	15,683
6	Victor J. Daniel Jr. Electric Generating Plant, Escatawpa, MS 39552	30.533944	88.55636	31,767	12,928
7	R.D. Morrow Generating Plant, Purvis, MS 39475	31.216333	89.395333	12,465	7,896
8	Big Cajun II Power Plant, New Roads, LA 70760	30.726667	91.366944	44,556	–

Fig. 6 HYSPLIT-generated SO$_2$ concentration (μg m^{-3}) averaged between 0 and 100 m levels and integrated for 24-h period between 0100 UTC of 18 June 2009 and 0100 UTC of 19 June 2009 sourced from the three identified coal-fired power plants
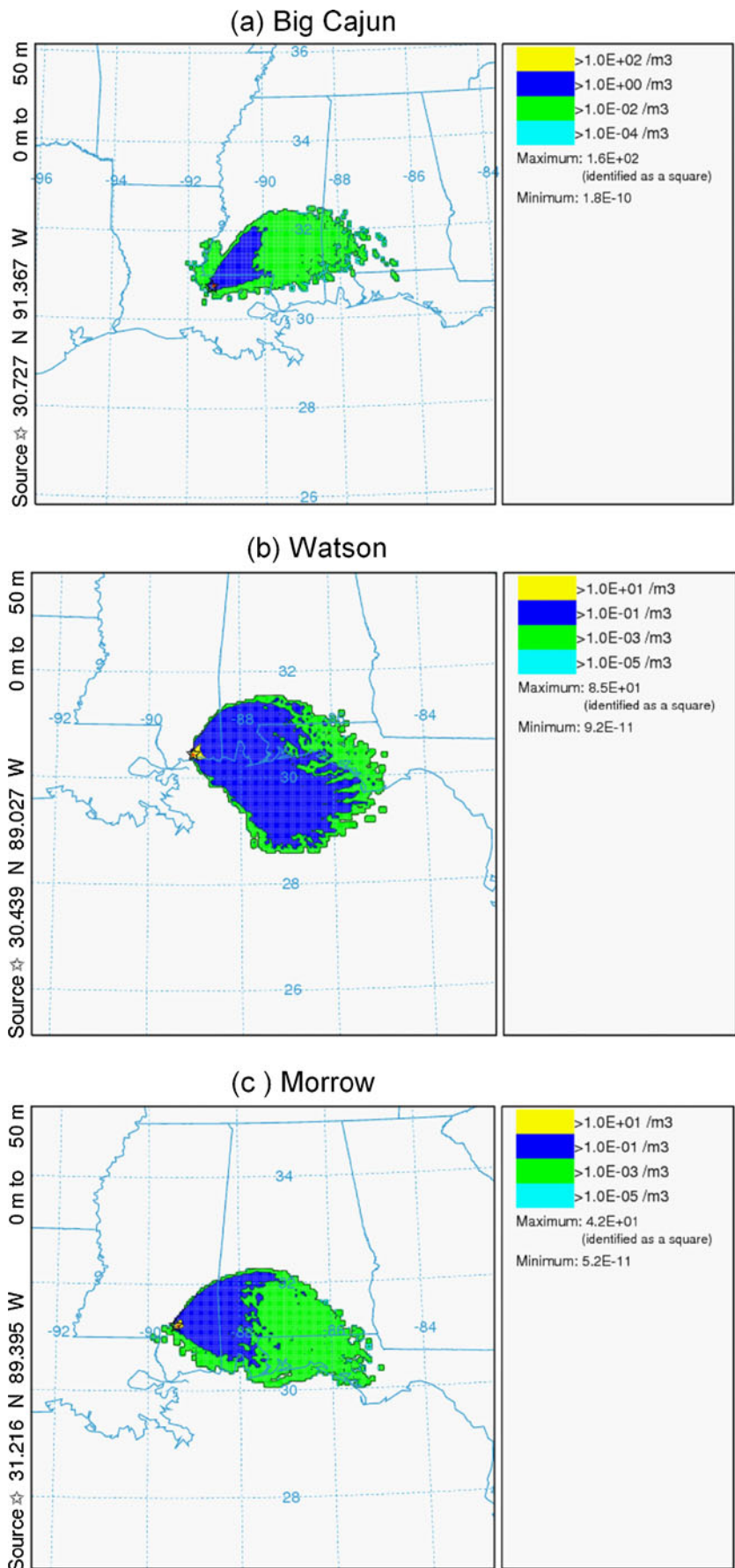
Table 3 Model-simulated concentrations of SO$_2$ (µg m^{-3}) from different power plants along with observations at HCHS

Time		Observed SO$_2$	Model-simulated SO$_2$			
From	To		Watson	Morrow	Cajun	Total
6/17/2009 20:00	6/18/2009 2:00	7.14	0.0	0.0	0.0	0.0
6/18/2009 2:00	6/18/2009 8:00	6.91	0.0	0.0	0.0	0.0
6/18/2009 8:00	6/18/2009 14:00	6.57	0.0	0.0	0.0	0.0
6/18/2009 14:00	6/18/2009 20:00	6.48	0.0	0.0	0.0	0.0

and the clockwise divergent flow over the model domain under the influence of a high pressure system at both the synoptic times. The above description of the model-simulated wind flow at 0100 and 1300 CST (local time) represents the coastal circulations associated with midnight cool and stable and noontime thermal induced convective boundary layer. The simulated wind fields at the two synoptic times of 0100 and 1300 CST are noted to have very good correspondence with NAM analysis. The differences in the wind flow regimes between 0600 and 1800 UTC (0100 and 1300 CST), which correspond to midnight and noon hours, indicate diurnal changes over the Gulf Coast region. The onset of sea breeze, as expected during the summer period along the coastal region, was distinctly indicated at 1300 CST, with strong sea breeze along the coastal regions, but the in-land extent of the sea breeze was contained due to the influence of the high pressure system. It is important to note that the model-simulated wind flow shows mesoscale features as compared to smooth wind flow in NAM analysis which emphasizes the need for high resolution wind flow simulation for application to dispersion computations. The simulated mesoscale characteristics of the wind flow along the coast line at 1800 UTC will have a significant impact on the computation of back trajectories and the forward dispersion using HYSPLIT. These results from ARW model integrations show that the adopted model dynamics and physics could generate the mesoscale circulations through interaction with high resolution (30″ data) topography and land use informatics.

Back trajectories

ARW model generated outputs at 1-h intervals for 48 h, from 02 to 23 UTC 17 June 2009; 00–23 UTC of 18 June

2009 and 00–01 UTC of 19 June 2009 were used as input to HYSPLIT model to produce 24 numbers of back trajectories at 1-h intervals starting from 0200 UTC of 18 June 2009 to 0100 UTC of 19 June 2009 each with duration of 24 h. In general, the transport of air masses over a regional scale (~1,000 km) takes 2–3 days (Chen et al. 2002). As the back trajectories in our study are reaching 300 km within 24 h (where the considered power plants are located), we have run the HYSPLIT for 24 h alone.

These back trajectories describe the Lagrangian path of the air parcels that culminate at the observation site in the 24-h period of 0200 UTC of 18 June to 0100 UTC of 19 June 2009. This procedure yielded 24 numbers of back trajectories at 1-h interval during the 24-h period from 02 UTC of 18 June to 01 UTC of 19 June 2009 and each with duration of 24 h. Each back trajectory describes the path of the particle traced backward for 24 h in time initiated at 1-h interval (i.e.) first trajectory as from 01 UTC of 19 to 01 UTC of 18 June, second as from 00 UTC of 19 to 00 UTC of 18 June etc., and 24th trajectory as from 02 UTC of 18 to 02 UTC of 17 June. This procedure was repeated for each observation site, and plots of the back trajectories from the two observation sites of HCHS and WSCA are presented in Fig. 5. From both the observation sites, the computed back trajectories show that the air parcels had paths distributed in the quadrant between south and west. The paths were mostly confined to the heights below 1.0 km, within the planetary boundary layer. These were collated with all the power plants that were located within a 300-km radius of the two observation sites, HCHS and WSCA (Fig. 2).

The list of the coal-fired power plants, their locations, and the annual emission rates is given in Table 2. The back trajectories distinctly indicated emission source locations to be in the quadrant between south and west, all pointing the

Table 4 Model-simulated concentrations of NO$_x$ (µg m^{-3}) from different power plants along with observations at HCHS

Time		Observed HNO$_3$	Model-simulated NO$_x$			
From	To		Watson	Morrow	Cajun	Total
6/17/2009 20:00	6/18/2009 2:00	1.47	0.0	0.0	0.0	0.0
6/18/2009 2:00	6/18/2009 8:00	1.03	0.0	0.0	0.0	0.0
6/18/2009 8:00	6/18/2009 14:00	3.33	0.0	0.0	0.0	0.0
6/18/2009 14:00	6/18/2009 20:00	3.51	0.0	0.0	0.0	0.0

NO$_x$ emission data is not available for Cajun Power Plant

Table 5 Model-simulated concentrations of SO_2 ($\mu g \ m^{-3}$) from different power plants along with observations at WSAP

Time		Observed SO_2	Model-simulated SO_2			
From	To		Watson	Morrow	Cajun	Total
6/17/2009 20:00	6/18/2009 2:00	8.89	0.0	0.0	0.0	0.0
6/18/2009 2:00	6/18/2009 8:00	8.2	0.0	0.0	0.0	0.0
6/18/2009 8:00	6/18/2009 14:00	7.18	0.0	0.134	0.0	0.134
6/18/2009 14:00	6/18/2009 20:00	6.16	0.0	0.0	0.235	0.235

origination of parcels from land on west-side and from sea on south-side (i.e.) Gulf of Mexico. Specifically, Watson, Cajun, and Morrow power plants are identified to be possible land sources as located within the path of back trajectories. These three identified sources were used for computing forward atmospheric dispersion of SO_2 and NO_x, which are known to be precursors of the observed sulfate and HNO_3.

Atmospheric dispersion

With the objective of assessing the relative contributions from each of the three identified sources from the back trajectory analysis, HYSPLIT model was used in forward mode driven by ARW model inputs. The annual emission rates for the coal-fired power plants are taken from 2006 US EPA data (http://www.epa.gov/) and are given in Table 2. As continuous monitoring data for these sources is not available for the study period, these annual emission rates were converted to hourly emission rates and assumed to be representative for the period of this study.

HYSPLIT model was run in the forward mode, driven by the ARW model-generated atmospheric fields at 1-h interval and the hourly emission rates, starting from each of the three identified coal-fired power plants to produce the 24-h atmospheric dispersion separately for SO_2 and NO_x. To facilitate an estimation of the relative contribution from the different sources for the observations at HCHS and WSAP in the Gulfport region, the pollutant concentration was averaged for the vertical layer immediately above the surface between 0 and 100 m, assuming that there will be uniform and rapid vertical mixing in this lowest turbulent layer. The computed near-surface pollutant concentrations are time

dependent. The forward 24-h atmospheric dispersions from the three sources for SO_2 alone are presented (Fig. 6) as the dispersion pattern is the same for SO_2 and NO_x and as the magnitude alone differs by relative fraction. The spatial patterns are similar for both the SO_2 and NO_x pollutants as both are treated as species of gas with dry deposition. The general pattern of dispersion from all the sources is noted to be towards east/northeast, under the prevailing wind flow of southwesterly/westerly relative to the observation sites, as noted earlier in this section (Fig. 4). The pattern of the pollutant dispersion is like a plume slowly expanding in the forward direction following the wind flow. The dispersive plume is due to the low magnitude of the wind speed (2–5 m s^{-1}). This kind of wide and dispersive plume is expected under low wind speeds as compared to narrow and longer dispersion under the influence of high wind speed conditions. In addition, the concentrations of the pollutants from all the other five coal-fired power plants were also examined and the dispersion patterns are noted to be different as they are related to the differences in the wind flow regimes (not shown).

The contributions from each of the three power plants to HCHS and WSAP are computed for the 6-h periods during 0100 UTC of 18 June 2009 to 0100 UTC of 19 June 2009 using the computational facility available with HYSPLIT 4.9 package and are presented in Tables 3, 4, 5, and 6. The computations show that on this day (18 June 2009), while Big Cajun and Morrow plants contribute only to a smaller extent <0.235 $\mu g \ m^{-3}$ for WSAP location, none of three sources contribute for the observations at HCHS though these two sites are 65 km apart.

These results are to be interpreted with caution as daily values of emissions based on 2006 data are used

Table 6 Model-simulated concentrations of NO_x ($\mu g \ m^{-3}$) from different power plants along with observations at WSAP

NO_x emission data is not available for Cajun Power Plant

Time		Observed HNO_3	Model-simulated NO_x		
From	To		Watson	Morrow	Total
6/17/2009 20:00	6/18/2009 2:00	1.12	0.0	0.0	0.0
6/18/2009 2:00	6/18/2009 8:00	1.37	0.0	0.0	0.0
6/18/2009 8:00	6/18/2009 14:00	2.29	0.0	0.085	0.085
6/18/2009 14:00	6/18/2009 20:00	1.77	0.0	0.0	0.0

for the computations and there could be temporal variations. Underlying reasons for observations at HCHS and WSAP are to be examined more in detail to find some other local sources which could have contributed for the observed concentrations. For example, as mobile sources in urban areas are expected to contribute significantly to $PM_{2.5}$ the New Orleans metro region (transportation) which falls in the path of the back trajectories may also be a potential contributor.

Conclusions

ARW model simulated the diurnal variations of the wind flow over the Mississippi Gulf Coast study region at the 4-km resolution agreeing with NAM-12 km analyses. The model-simulated wind flow has shown the generation of the land and sea breezes along the coast line under the influence of an existing high pressure system during the study period. The model has simulated the mesoscale characteristics along the coast line, not shown in NAM-12 km analyses. These results indicate the usefulness of the methodology of source identification through back trajectories and source attribution of emissions and the strong influence of the atmospheric flow patterns on pollutant dispersion. This study further emphasizes the need for accurate simulation of atmospheric flow fields at reasonably high temporal and spatial resolution.

In the present study, modeled SO_2 concentration contributes only 4% (0.235 out of 6.16 µg m^{-3}) of observations which suggests that SO_2 concentration is dominated by other sources than the coal-fired power plants. The concentrations at both the monitoring stations HCHS and WSAP which are 65 km apart recorded maximum daily averages between 5 and 8 µg m^{-3} for sulfate. Moderate events like this with good spatial variability are considered as characteristic of major contribution from local sources (Allen 2002). Further, the 24-h back trajectories predict synoptic scale winds come in the quadrant between south and west due to which air is advected from the Gulf of Mexico. Due to increasing activity in diesel-powered heavy duty vehicle (ship) over the Gulf of Mexico (as 60% of US energy imports are from this area) and ports around, diesel oil emissions from this area may also contribute to precursors SO_2 and NO_x of P.M.$_{2.5}$ as reported by Fraser et al. (2003). The source attribution from the Gulf of Mexico could also be due to the diurnal Gulf breeze which is represented in the present mesoscale simulation. The land breeze prevailing during the night time would carry the land-borne precursor pollutants on to the sea, while the Gulf breeze which sets in during the day time would recirculate the pollutants from the sea back to the land region, thus representing the Gulf of Mexico as a virtual pollutant source.

Normally, events with maximum daily average concentrations, typically ranging between 40 and 65 µg m^{-3}, with less spatial variability represent regional sources. These are not only important from an acute exposure health perspective but also in determining compliance with the NAAQS. Study of such episodic events, using this kind of WRF–HYSPLIT integrated modeling approach, will provide better understanding of sources and their relative contribution, for which monitoring data of longer time periods with larger spatial networks is needed. As a continuation of this study, we are taking up critical analysis of $PM_{2.5}$ episodic events over the Gulf Coast, MS region.

References

Allen D (2002) Gulf coast aerosol research and characterization program (Houston Supersite). Report for the Environmental Protection Agency, Center for Energy and Environmental Resources, The University of Texas at Austin, Austin, Texas, USA, July. Available at http://eosweb.larc.nasa.gov/PRODOCS/narsto/document/EPA_SS_Houston_Final_Report.pdf

Anjaneyulu Y, Venkata Srinivas C, Jayakumar I, Hariprasad J, Baham J, Patrick C, Young J, Hughes R, White LD, Hardy MG, Swanier S (2008) Some observational and modeling studies of the coastal atmospheric boundary layer at Mississippi Gulf coast for air pollution dispersion assessment. Int J Environ Res Public Health 5:484–497

Anjaneyulu Y, Venkata Srinivas C, Hariprasad D, White LD, Baham JM, Young JH, Hughes R, Patrick C, Hardy MG, Swanier S (2009) Simulation of atmospheric dispersion of air-borne effluent releases from point sources in Mississippi Gulf Coast with different meteorological data. Int J Environ Res Public Health 6:1055–1074

Challa VS, Jayakumar I, Baham JM, Hughes R, Patrick C, Young J, Rabbarison M, Swanier S, Hardy MG, Anjaneyulu Y (2008) Sensitivity of atmospheric dispersion simulations by HYSPLIT to the meteorological predictions from a mesoscale model. Environ Fluid Mech 8:367–387

Challa VS, Jayakumar I, Baham JM, Hughes R, Patrick C, Young J, Rabbarison M, Swanier S, Hardy MG, Anjaneyulu Y (2009) A simulation study of mesoscale coastal circulations in Mississippi Gulf coast for atmospheric dispersion. Atmos Res 91:9–25

Chen F, Dudhia J (2001) Coupling an advanced land-surface/hydrology model with the Penn State/NCAR MM5 modeling system. Part I: model description and implementation. Mon Weather Rev 129:569–585

Chen LWA, Doddridge BG, Dickerson RR, Chow JC, Henry RC (2002) Origins of fine aerosol mass in the Baltimore–Washington corridor:

implications from observation, factor analysis, and ensemble air parcel back trajectories. Atmos Environ 36:4541–4554

Draxler RR (2006) The use of global and mesoscale meteorological model data to predict the transport and dispersion of tracer plumes over Washington, D.C. Weather Forecast 21:383–394

Draxler RR, Hess GD (1997) Description of the HYSPLIT_4 modeling system. NOAA Tech. Memo. ERL ARL-224, pp 24

Draxler RR, Hess GD (1998) An overview of the HYSPLIT_4 modeling system for trajectories, dispersion and deposition. Aust Meteorol Mag 47:295–308

Draxler RR, Rolph GD (2010) HYSPLIT (HYbrid Single-Particle Lagrangian Integrated Trajectory) Model. NOAA Air Resources Laboratory, Silver Spring, MD. Available at NOAA ARL READY Website http://ready.arl.noaa.gov/HYSPLIT.php

Dudhia J (1989) Numerical study of convection observed during the Winter Monsoon Experiment using a mesoscale two-dimensional model. J Atmos Sci 46:3077–3107

Fraser MP, Yue ZW, Buzcu B (2003) Source apportionment of fine particulate matter in Houston, TX, using organic molecular markers. Atmos Environ 37:2117–2123

Hong SY, Dudhia J, Chen SH (2004) A revised approach to ice microphysical processes for the bulk parameterization of clouds and precipitation. Mon Weather Rev 132:103–120

Hong SY, Noh Y, Dudhia J (2006) A new vertical diffusion package with an explicit treatment of entrainment processes. Mon Weather Rev 134:2318–2341

Jin H, Raman S (1996) Dispersion of an elevated release in a coastal region. J Appl Meteorol 35:1611–1624

Kain JS, Fritsch JM (1993) In: Emanuel KA, Raymond DJ (eds) Convective parameterization for mesoscale models: the Kain–Fritsch scheme. The representation of cumulus convection in numerical models. Amer Meteor Soc 246 pp

Kantha LH, Clayson CA (2000) Small scale processes in geophysical fluid flows, vol. 67, International Geophysics Series. Academic, San Diego, p 883

Kotroni V, Kallos G, Lagouvardos K, Varinou M (1999) Numerical simulations of the meteorological and dispersion conditions during an air pollution episode over Athens, Greece. J Appl Meteorol 38:432–447

Lu R, Turco RP (1995) Air pollutant transport in a coastal environment II. Three-dimensional simulations over Los Angeles Basin. Atmos Environ 29:499–1518

Mlawer EJ, Taubman SJ, Brown PD, Iacono MJ, Clough SA (1997) Radiative transfer for inhomogeneous atmosphere: RRTM, a validated correlated-k model for the longwave. J Geophys Res 102:16663–16682

Moran MD, Pielke RA (1996) Evaluation of a mesoscale atmospheric dispersion modeling system with observations from the 1980 Great Plains mesoscale tracer field experiment. Part II: dispersion simulations. J Appl Meteorol 35:308–329

Myles L, Dobosy RJ, Meyers TP, Pendergrass WR (2009) Spatial variability of sulfur dioxide and sulfate over complex terrain in East Tennessee, USA. Atmos Environ 43:3024–3028

Parkhurst WJ, Tanner RL, Weatherford FP, Valente RJ, Meagher JF (1999) Historic $PM_{2.5}/PM_{10}$ concentrations in the Southeastern United States—potential implications of the revised particulate matter standard. J Air Waste Manage 49:1060–1067

Pendergrass WR, Latoya M, Vogel CA, Dodla VBR, Dasari HP, Yerramilli A, Baham JM, Hughes R, Patrick C, Young J, Swanier SJ (2010) Analysis and prediction of the atmospheric boundary layer characteristics during the NOAA/ARL–JSU meteorological field experiment, summer—2009. Proceedings of the 90th Annual Meeting of the American Meteorological Society Conference held in Atlanta, GA, USA, 17–21 Jan

Pendergrass WR, Latoya M, Vogel CA, Dodla VBR, Yerramilli A, Dasari HP, Srinivas CV, Baham JM, Hughes R, Patrick C, Young J, Swanier SJ (2010) Numerical prediction of atmospheric mixed layer variations over the Gulf Coast region during NOAA/ARL JSU meteorological field experiment summer 2009—sensitivity to vertical resolution and parameterization of surface and boundary layer processes. Proceedings of the 90th Annual Meeting of the American Meteorological Society Conference held in Atlanta, GA, USA, 17–21 Jan

Physick WL, Abbs DJ (1991) Modeling of summertime flow and dispersion in the coastal terrain of Southeastern Australia. Mon Weather Rev 119:1014–1030

Pielke RA, Lyons WY, McNider RT, Moran MD, Moon DA, Stocker RA, Walko RL, Uliasz M (1991) Regional and mesoscale meteorological modeling as applied to air quality studies. In: van H Dop, Steyn DG (eds) Air pollution modeling and its application VIII. Plenum, New York, pp 259–289

Segal M, Pielke RA, Arritt RW, Moran MD, Yu CH, Henderson D (1988) Application of a mesoscale atmospheric dispersion modeling system to the estimation of SO_2 concentrations from major elevated sources in Southern Florida. Atmos Environ 22:1319–1334

Skamarock WC, Klemp J, Dudhia J, Gill DO, Barker DM, Wang W, Powers JG (2008) A description of the advanced research WRF version 2. NCAR technical note, NCAR/TN-468+STR. Mesoscale and Microscale Meteorology Division, National Center for Atmospheric Research, Boulder, CO, USA

United States Environmental Protection Agency (2004) The particle pollution report current understanding of air quality and emissions through 2003. US Environmental Protection Agency, Office of Air Quality Planning and Standards Emissions, Monitoring, and Analysis Division, Research Triangle Park, NC, USA. Report No. EPA 454-R-04-002, December

Wang G, Ostoja-Starzewski M (2004) A numerical study of plume dispersion motivated by a mesoscale atmospheric flow over a complex terrain. Appl Math Model 28:957–981

Weber R, Orsini D, Duan Y, Baumann K, Kiang CS, Chameides W, Lee YN, Brechtel F, Klotz P, Jongejan P, Ten Brink H, Slanina J, Boring CB, Genfa Z, Dasgupta PK, Hering S, Stolzenburg M, Dutcher DD, Edgerton ES, Hartsell BE, Solomon P, Tanner RL (2003) Intercomparison of near real time monitors of $PM_{2.5}$ nitrate and sulfate at the U.S. Environmental protection agency Atlanta supersite. J Geophys Res 108:8421

Zhang Y, Wen XY, Wang K, Vijayaraghavan K, Jacobson MZ (2009) Probing into regional O_3 and particulate matter pollution in the United States: 2. An examination of formation mechanisms through a process analysis technique and sensitivity study. J Geophys Res 114:D22305. doi:10.1029/2009JD011900